Scilight

Smart Chemical Engineering

https://www.sciltp.com/journals/sce

Article

Check for updates

Machine Learning-Driven Prediction of Li^+/Mg^{2+} Separation Performance in Crown Ether-Modified Graphene Oxide Membranes

Mengmeng Ge [1], Chunlei Wei [2], Yi Song [1], Timing Fang [1,*] and Xiaomin Liu [1,*]

[1] College of Chemistry and Chemical Engineering, College of Materials Science and Engineering, Qingdao University, Qingdao 266071, China
[2] Institute of Zhejiang University-Quzhou, Quzhou 324000, China
* Correspondence: tmfang@qdu.edu.cn (T.F.); liuxiaomin@qdu.edu.cn (X.L.)

How To Cite: Ge, M.; Wei, C.; Song, Y.; et al. Machine Learning-Driven Prediction of Li^+/Mg^{2+} Separation Performance in Crown Ether-Modified Graphene Oxide Membranes. *Smart Chemical Engineering* **2026**, *2*(2), 7. https://doi.org/10.53941/sce.2026.100007

Received: 18 May 2026
Revised: 15 June 2026
Accepted: 16 June 2026
Published: 25 June 2026

Abstract: The efficient separation of Li^+ from Mg^{2+} in salt lake brines is a critical bottleneck for sustainable lithium extraction. Crown ether (CE)-modified graphene oxide (GO) membranes offer enhanced ion selectivity via specific host–guest recognition. However, their performance is governed by multiple structural descriptors, including CE content, interlayer spacing, asymmetric charge, and membrane inclination, which are difficult to optimize using molecular dynamics (MD) simulations alone due to high computational cost and limited quantitative predictive capability. To address this challenge, this study integrates MD simulation with machine learning (ML) to construct a high-accuracy proxy model for predicting the Li^+/Mg^{2+} separation performance of CE-functionalized GO membranes. Using Random Forest (RF) and Extreme Gradient Boosting (XGBoost) regression models, we established quantitative relationships between four key structural descriptors and three performance indicators: water flux, Li^+ permeability, and Mg^{2+} retention rate. RF outperforms XGBoost, achieving high test accuracy. Feature importance reveals distinct mechanisms: water flux is governed by interlayer spacing and membrane inclination, Li^+ permeability is co-determined by interlayer spacing and CE number. Mg^{2+} retention depends mainly on CE grafts and non-uniform charge distribution, reflecting synergy between Donnan effect and specific recognition. Moreover, interactive effects among structural parameters are identified, CE number couples with spacing to enhance Li^+ permeability, and with non-uniform charge to boost Mg^{2+} retention, providing quantitative evidence for the proposed separation mechanisms. Multi-objective optimization yields two membrane schemes, the optimally balanced design achieves both high selectivity and competitive flux, showing strong application potential. This study not only overcomes the limitations of conventional MD simulations but also establishes a data-driven framework for the rational design and efficient optimization of high-performance lithium-selective membranes.

Keywords: lithium-magnesium separation; molecular dynamics simulation; machine learning; structure–performance relationship

1. Introduction

Lithium possesses both energy and strategic value. With its high electrochemical activity, good conductivity, excellent ductility, and high specific heat capacity, it is widely used in various fields such as new energy batteries,

aerospace, biomedicine, glass and ceramics [1–3]. Among them, lithium-ion batteries account for approximately 50% of the global lithium consumption market. With the rapid development of electric vehicles and electronic devices, the demand for lithium continues to rise, becoming a key raw material supporting the green energy transition [4–6]. It is expected to grow significantly in the future. Membrane separation technology is widely used in water treatment, resource recovery, gas separation and resource extraction due to its high efficiency, low energy consumption and good selectivity. In recent years, two-dimensional materials such as graphene oxide have shown great potential in the field of ion sieving due to their high specific surface area, adjustable interlayer spacing and good mechanical stability [7–9]. Traditional graphene oxide (GO) membranes have problems such as insufficient mechanical strength, limited selectivity and poor long-term stability, so improving their comprehensive separation performance has become the current research focus [10].

The GO membrane can achieve the basic separation of Li^+/Mg^{2+}, but Li^+ and Mg^{2+} are highly similar in hydration characteristics and chemical properties, and the efficient separation of the two has become a core challenge in the process of extracting lithium from salt lakes [11,12]. Pristine GO is difficult to achieve the efficient separation of Li^+/Mg^{2+}. Crown ether (CE), as a class of heterocyclic ligands with specific ion recognition function [13], provide a feasible solution to this problem. CE can form host-guest complexes with metal ions through ion-dipole interactions and exhibit excellent selectivity for Li^+ and other cations by relying on the "size matching" effect [14,15]. In previous work, to improve the single electrostatic interaction in GO, specific recognition sites (15-crown-5, 15C5) were introduced to effectively improve the ion selectivity [16]. In addition, by breaking the uniformity limitation of the channel-intra-pathway effect and introducing asymmetric charges and structures, the membrane separation performance was also improved [17,18]. From the above analysis, it can be found that the content of CE, interlayer spacing, non-uniform charge density and inclination angle will all become key factors affecting the membrane separation performance. However, MD simulation has inherent limitations: on the one hand, the simulation process requires a significant amount of computing resources, making it difficult to achieve efficient screening of multiple parameters and large samples, and unable to quickly explore the quantitative correlations between membrane structure and performance under different CE modification conditions; on the other hand, MD simulation focuses on the qualitative description of microscopic mechanisms and is difficult to establish a precise quantitative relationship between membrane structure descriptors and macroscopic separation performance, which restricts the efficient design and optimization of CE-modified GO membranes.

With the rapid penetration of artificial intelligence technology in the field of materials science, machine learning (ML) has become an efficient tool for solving complex problems such as material design and performance prediction [19,20]. In recent years, machine learning methods have demonstrated strong data mining and performance prediction capabilities in the field of membrane separation. Researchers have begun to systematically apply ML to membrane material design, performance prediction, and separation mechanism analysis, providing data-driven theoretical guidance for the rational design of high-performance separation membranes [21,22]. In the field of ion selective separation, Lu et al. [23] used integrated machine learning to reveal the mechanism of Zeta potential and pore size jointly regulating ion sieving in polyamide nanofiltration membranes. For salt lake lithium-magnesium separation, Sun et al. [24] constructed a prediction model based on literature data and found that the $MgCl_2$ retention rate is a key comprehensive indicator determining the selectivity of Li^+/Mg^{2+} ions, emphasizing the necessity of multi-factor coupling modeling. In the field of two-dimensional membrane materials, Bonnet et al. [25] combined machine learning molecular dynamics to analyze the sieving mechanism of Li^+, Na^+, and K^+ in corannulene-functionalized graphene membranes, providing a theoretical reference for this research. At the methodological level, Ignacz et al. [26] systematically reviewed the progress of ML in membrane science, emphasizing the importance of feature engineering and model interpretability, providing methodological guidance for the model construction of this chapter. In summary, although machine learning has been used to predict key performance indicators such as membrane permeability and selectivity in two-dimensional separation membranes in this field, for corannulene-modified GO membranes, machine learning research combining membrane structure descriptors and multiple performance indicators is remains limited, especially lacking systematic exploration of the quantitative correlation between membrane non-homogeneous structure parameters and performance indicators such as Li^+ permeability and Mg^{2+} retention rate.

Based on this, this work takes the GO membrane modified by CE as the research object and conducts molecular dynamics simulation on the Li^+/Mg^{2+} separation process. Four core membrane structure descriptors, namely the number of CE, the non-uniform charge of the membrane, the membrane inclination angle, and the interlayer spacing, are selected as input features. Three key performance indicators, namely water flux, Li^+ permeability, and Mg^{2+} retention rate, are taken as label values to construct two regression models, namely Random Forest (RF) and Extreme Gradient Boosting (XGBoost). Through dataset division, model training, and hyperparameter optimization, accurate prediction of multiple performance indicators of the CE-modified GO

membrane is achieved. The influence weights of each structure descriptor on membrane performance are analyzed, and the quantitative rules of CE regulating the performance of GO membranes are revealed. This provides efficient theoretical tools and technical support for the rational design, performance optimization, and industrial application of CE-modified GO membranes.

2. Models and Methods

Molecular Models

The separation model adopted in this paper is consistent with our previous research work [16]. As shown in Figure 1, a GO sheet model with a size of 30 Å × 32 Å was constructed using the Materials Studio (MS) software. The model considered the random distribution of oxygen-containing groups (hydroxyl and epoxy groups) on both sides of the GO sheet layer, with the molar ratio of hydroxyl to epoxy groups set at 1:1, and the oxidation degree (R_0) fixed at 10% (defined as R_0 = Eo/Ec, where Eo and Ec are the number of oxygen and carbon atoms in the system) [27]. By carboxylating or amidoating the GO sheet, functionalized GO nanosheets with opposite electronegativity were prepared; these two nanosheets were stacked in parallel to construct a "double-sided heterogeneous electrification" nanochannel membrane. The left side of the nanochannel was the feed side, where 5200 water molecules, 24 Mg^{2+}, 24 Li^{+}, and 72 Cl^{-} were pre-filled to construct a 0.5 M $MgCl_2$ and LiCl mixed solution system [17]; the right side of the channel was the permeation side, and initially only 520 water molecules were filled. To simulate the pressure-driven membrane separation process, rigid plates composed of helium atoms were set at the leftmost position on the feed side and the rightmost position on the permeation side as pressure application interfaces. The left pressure plate applied a pressure of 110 MPa, and the right one applied 10 MPa, forming a net pressure gradient of 100 MPa to simulate the working pressure environment of the actual nanofiltration process [28].

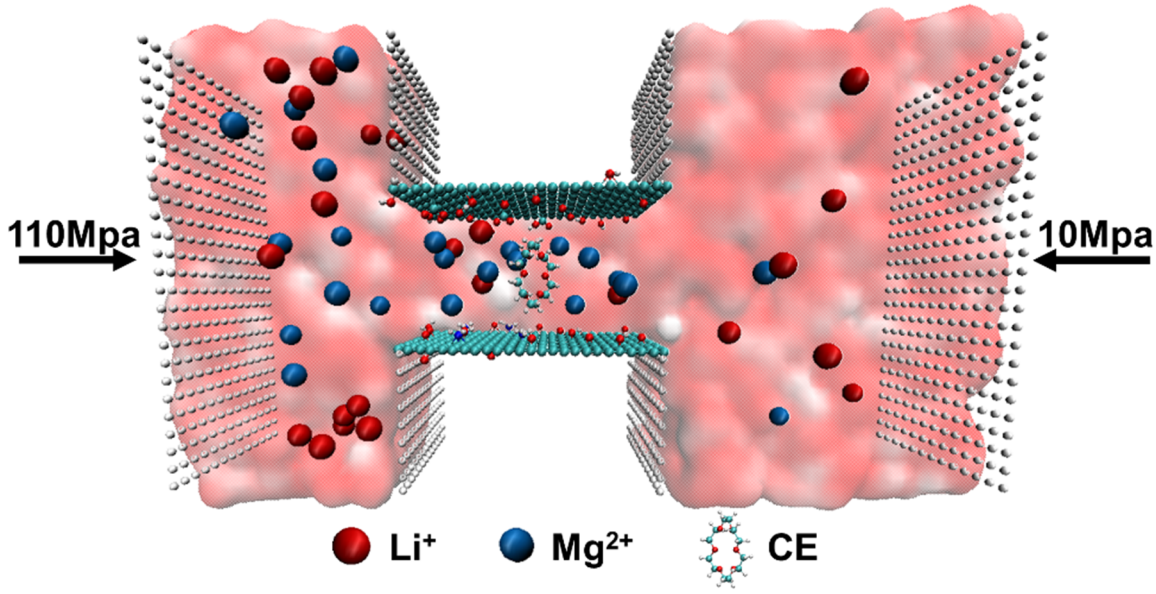

Figure 1. Schematic diagram of a simulation system for Li^{+}/Mg^{2+} separation. All components are labeled in the figure and Cl^{-} is omitted for clarity.

All molecular dynamics simulations were completed using the Large-scale Atomic/Molecular Massively Parallel Simulator (LAMMPS) [29]. Water molecules were described using the SPC/E model [30], the atomic interaction parameters of Li^{+}, Mg^{2+}, and GO were set using the OPLS-AA force field [31,32], the force field parameters of the CE molecule were set according to the reliable research results reported previously. Non-bonded interactions were described using the 12–6 Lennard-Jones potential function, with the short-range interaction cutoff radius set at 12.5 Å; electrostatic interactions were calculated using the particle-particle-grid (PPPM) method, with the cutoff radius set at 12 Å. The simulation was conducted in the canonical ensemble (NVT), and the temperature was controlled by the Nosé-Hoover heat bath at 303.15 K [33]. The simulation time step was set at 1 fs, and simulation data was collected every 1 ps, with a total simulation duration of 30 ns to ensure the system reached thermodynamic equilibrium and to obtain reliable statistical results.

The dataset consists of a total of 240 samples, covering the GO membrane structure and corresponding performance parameters under different CE modification conditions, as shown in Table 1. Four membrane

structure descriptors (the number of CE, the non-uniform charge of the membrane, the membrane inclination angle, and the interlayer spacing) are used as input features, while water flux, Li^+ permeability, and Mg^{2+} retention rate are taken as label values. A multi-output regression model is constructed for prediction. The specific selection parameters are as follows (Table 2):

1. Number of Crown Ethers (Nce): The total number of functionalized CE molecules inserted between the GO membrane layers (15Cs), ranging from 0 to 2, with an interval of 1, corresponding to different CE loading amounts, which mainly reflects the regulatory effect of the introduced CE molecules on the membrane structure and performance, consistent with the research logic of CE content in the second chapter;
2. Charge Content (Pcharge): The degree of non-uniformity of the non-uniform charge in the GO membrane layer, ranging from 0% to 75%, reflecting the non-uniformity of the charge distribution within the membrane, directly related to the direct regulation of the Donnan effect intensity;
3. Inclination Angle (tilt-angle): The angle between the GO nanosheets layer and the normal direction of the membrane surface (unit: °), ranging from −5° to 10°, with an interval of 5°, reflecting the regularity of membrane layer stacking, and an excessive inclination angle will cause the interlayer channels to twist, affecting the ion transmission efficiency;
4. Interlayer Spacing (gap): The average distance between the GO membrane layers (unit: Å), ranging from 10 to 18 Å, with an interval of 2 Å, determined by the spatial size of the CE molecules and the interaction between the GO layers, and this parameter is the core structural parameter affecting the ion size retention rate and transmission rate.

Three key separation performance indicators of the CE-modified GO membrane in the lithium extraction from salt lakes scenario are selected as model label values, namely water flux (Flux_water), which reflects the membrane's mass transfer efficiency and is one of the core indicators for membrane industrial application; Li^+ permeability (P_Li^+), which reflects the transmission rate of Li^+ in the membrane and is directly related to the Li^+ separation efficiency of the membrane; Mg^{2+} retention rate (R_Mg^{2+}), which reflects the membrane's retention ability of Mg^{2+}, is a key indicator for evaluating the Li^+/Mg^{2+} separation performance.

Table 1. The selected structural descriptors and label values.

Structure Parameter	Membrane Performance Indicators
Number of CE (Nce)	Water flux (Flux_water)
Electronegativity content (Pcharge)	Li^+ permeability (P_Li^+)
Angle of inclination (tilt-angle)	Mg^{2+} retention rate (R_Mg^{2+})
Interlayer spacing (gap)	

Table 2. The specific selection parameters of membrane structure descriptors.

Nce	Pcharge	Tilt-Angle	Gap
0	0%	0°	10 Å
1	25%	5°	12 Å
2	50%	10°	14 Å
	75%	−5°	16 Å
			18 Å

To eliminate the dimensional differences between different features and label values (such as the unit of interlayer spacing being Å, the number of CE being an integer, and water flux being $L \cdot m^{-2} \cdot h^{-1} \cdot bar^{-1}$), and to avoid overemphasizing the features with large numerical values during the model training process, which may affect the prediction accuracy of the model. All input features and label values were standardized, using the Z-score standardization method [34,35], convert all features and label values into standardized data with a mean of 0 and a standard deviation of 1, eliminating the influence of dimensions. The calculation formula is as shown in Equation (1):

$$x_{norm} = \frac{x - \mu}{\sigma} \tag{1}$$

Among them, x_{norm} represents the standardized data, x is the original data, μ is the mean of the feature or label, and σ is the standard deviation of the feature or label. After the standardization process, all data are at the same magnitude, thereby ensuring the fairness and accuracy of model training. At the same time, outliers in the dataset are detected and handled. Using the 3σ criterion, abnormal samples are eliminated (a total of 3 groups of outliers were removed, and 237 valid samples were retained), ensuring the reliability of the dataset. The 237 valid samples after preprocessing are randomly divided into a training set and a test set, with a ratio of 8:2, that is, 190

samples are used for model training and 47 samples are used for model testing. The division process is carried out using a fixed random seed (seed = 42) [36], ensuring the reproducibility of the division results and avoiding distortion in model performance evaluation due to sample division bias.

Two classic ensemble learning regression models—Random Forest (RF) and Extreme Gradient Boosting (XGBoost) were selected to construct a prediction model for the separation performance of GO membranes modified with CE. Both models have strong nonlinear fitting ability, anti-overfitting ability and interpretability, and are suitable for small-sample, multi-feature, and multi-output regression problems [37,38]. They have been widely applied in the field of material performance prediction and can meet the research requirements of this chapter.

Random Forest is an ensemble learning method based on the Bagging strategy [39]. By constructing multiple decision trees and integrating their prediction results, it effectively reduces model variance and prevents overfitting. Each tree is trained using bootstrap sampling from the original training set, and during node splitting, some features are randomly selected for evaluation. For regression tasks, RF outputs the arithmetic mean of the predictions from all decision trees.

XGBoost is an ensemble learning method based on the Boosting strategy [40]. By iteratively adding weak learners (usually decision trees), each round of training focuses on the residuals from the previous round, gradually reducing model bias. XGBoost introduces regularization terms to control model complexity and supports parallel computing, with high prediction accuracy and robustness. For regression tasks, XGBoost uses the gradient boosting framework and the optimization objective was to minimize the mean squared error between the predicted values and the true values.

Model training and evaluation: For the three target variables of water flux, Li^+ permeability, and Mg^{2+} retention rate, separate RF and XGBoost regression models were trained independently. Grid search combined with 5-fold cross-validation was used to optimize the model's hyperparameters. To comprehensively evaluate the predictive performance of RF and XGBoost models, four commonly used regression model evaluation metrics were selected, namely coefficient of determination (R^2), root mean square error (RMSE), mean absolute error (MAE), and mean absolute percentage error (MAPE). The calculation formulas for each metric are as follows:

$$R^2 = 1 - \frac{\sum_{i=1}^{n}(y_i - \hat{y}_i)^2}{\sum_{i=1}^{n}(y_i - \bar{y})^2} \tag{2}$$

$$\mathrm{RMSE} = \sqrt{\frac{1}{n}\sum_{i=1}^{n}(y_i - \hat{y}_i)^2} \tag{3}$$

$$\mathrm{MAE} = \frac{1}{n}\sum_{i=1}^{n}|y_i - \hat{y}_i| \tag{4}$$

$$\mathrm{MAPE} = \frac{1}{n}\sum_{i=1}^{n}\left|\frac{y_i - \hat{y}_i}{y_i}\right| \times 100\% \tag{5}$$

Among them, y_i represents the actual value of the *i*-th sample, $\hat{y}_i$ represents the predicted value of the *i*-th sample by the model, $\bar{y}$ is the average value of the actual values of all samples, and n is the number of samples. The evaluation criteria for each indicator are as follows: The closer R^2 is to 1, the better the fitting effect of the model is, and the higher the consistency between the predicted value and the actual value; the smaller RMSE, MAE, and MAPE are, the smaller the prediction error of the model is, and the higher the prediction accuracy is [41]. By comparing the various evaluation indicators of the two models on the training set and the test set, the optimal prediction model is determined and used for subsequent performance prediction and feature influence analysis.

To reveal the influence weights of each membrane structure descriptor on the separation performance and to clarify the quantitative rules by which CE regulate the performance of GO membranes, the SHAP (SHapley Additive exPlanations) value analysis method was employed to conduct an interpretability analysis of the optimal machine learning model [42]. The SHAP value is based on the classic Shapley value in game theory and can quantify the contribution (positive or negative) of each input feature to the prediction result of each sample, intuitively reflecting the nonlinear relationship between the feature and the performance indicator [43]. This helps alleviate the "black box" problem of traditional machine learning models and provides a clear theoretical basis for the structural optimization of CE-modified GO membranes [44]. Through SHAP analysis, the following key information can be obtained: 1. The global importance ranking of each input feature, clearly identifying the main

structural parameters that affect the membrane separation performance; 2. The trend of the influence of a single feature on the performance indicator (positive or negative correlation); 3. The comprehensive influence of the interaction between different features on the performance indicator, providing support for multi-parameter collaborative optimization. However, it should be emphasized that the SHAP results only represent the interpretability of the machine learning model rather than a direct proof of physical causality, and thus the following discussion focuses on model-driven correlations rather than mechanistic conclusions.

3. Results and Discussion

3.1. Model Prediction Performance Evaluation

In this study, four membrane structure descriptors (the number of CE, the content of electronegativity, the tilt angle, and the interlayer spacing) were used as input features to construct an auxiliary model for simultaneously predicting three performance indicators (water flux, Li^+ permeability, and Mg^{2+} retention rate). The dataset (n = 240) was randomly divided into 80% for training and 20% for testing. For each target variable, RF and XGBoost regression models were trained separately, and the hyperparameters were optimized through grid search combined with five-fold cross-validation on the training set. To account for the wide dynamic range of water flux, the log1p transformation was applied during model fitting, and the inverse transformation was performed during prediction. For the two targets related to selectivity (Li^+ permeability and Mg^{2+} retention rate), considering that they are numerical values with limited effective digits measured in practice, we chose not to perform mathematical transformations but to retain the precision of the data itself as the objective for model learning. Overall, as shown in Figure 2, RF demonstrated strong predictive performance on the test set, with R^2 values of 0.881 for water flux, 0.950 for Li^+ permeability, and 0.943 for Mg^{2+} retention rate, indicating that the tree-based ensemble model can effectively capture the nonlinear relationship between membrane structure and separation performance. The RMSE values were 0.085 $L \cdot m^{-2} \cdot h^{-1} \cdot bar^{-1}$, 0.072 × 10^{-12} $m^2 \cdot s^{-1}$, and 0.92%, respectively, and the MAE values were 0.068 $L \cdot m^{-2} \cdot h^{-1} \cdot bar^{-1}$, 0.059 × 10^{-12} $m^2 \cdot s^{-1}$, and 0.75%, respectively, and the MAPE values were 2.15%, 1.98%, and 1.32%, all of which were relatively low level, indicating that the prediction error of the model was small and the prediction accuracy was high. In contrast, XGBoost was slightly less accurate in these two selectivity-related targets (test $R^2 \approx 0.91$ and 0.90) and in water flux (test $R^2 \approx 0.84$). The stability of the selected model was further verified through RepeatedKFold assessment (5 splits × 5 repetitions), the standard deviation of R^2 for the Random Forest (RF) model is ≤ 0.03 for all performance indicators, indicating low variance and stable generalization. The optimized hyperparameters for RF are n_estimators = 300 and max_depth = 10; for XGBoost, n_estimators = 200 and max_depth = 6. And the results showed that the average R^2 values under different data partitions were stable and had moderate variability, supporting the use of the random forest as the primary auxiliary model for subsequent multi-objective screening and Pareto-based optimization.

3.2. Model Interpretability Analysis

Taking the RF model as the research object, the SHAP analysis method was employed to quantify the influence weights of each input feature on the membrane separation performance, revealing the quantitative rules of CE in regulating the performance of GO membranes, and providing a theoretical basis for membrane structure optimization. Figure 3a–c presents the SHAP summary diagram of the RF model, which is used to explain the influence of membrane structure parameters on the Li^+ permeability, Mg^{2+} retention rate and water flux.

As shown in Figure 3, the interlayer spacing is the most crucial feature in all three tasks, indicating that the interlayer spacing is the most significant factor affecting water flux. This is because the interlayer spacing directly determines the effective size of the water molecule transmission channel, and the spatial effect plays a key role in the transmission of ions and water molecules. The larger the interlayer spacing, the smaller the resistance of water molecule transmission and the higher the water flux. For the permeability of Li^+, the number of inner CE has a significant contribution and is the core factor affecting the Li^+ permeability rate. This is because CE exhibit a specific recognition effect toward Li^+, indicating that the CE sites regulate the entry and migration of Li^+ through ion recognition and local coordination processes. The discreteness of the contribution direction suggests that this effect depends on the coordinated matching with other structural parameters. For Mg^{2+} retention, the results show that stronger confinement conditions are more conducive to improving the retention rate. Ge et al. [16] elucidated the atomic-scale mechanisms underlying CE-enhanced Li^+ transport, which corroborate our SHAP-based identification of CE number as the key descriptor for Li^+ permeability.

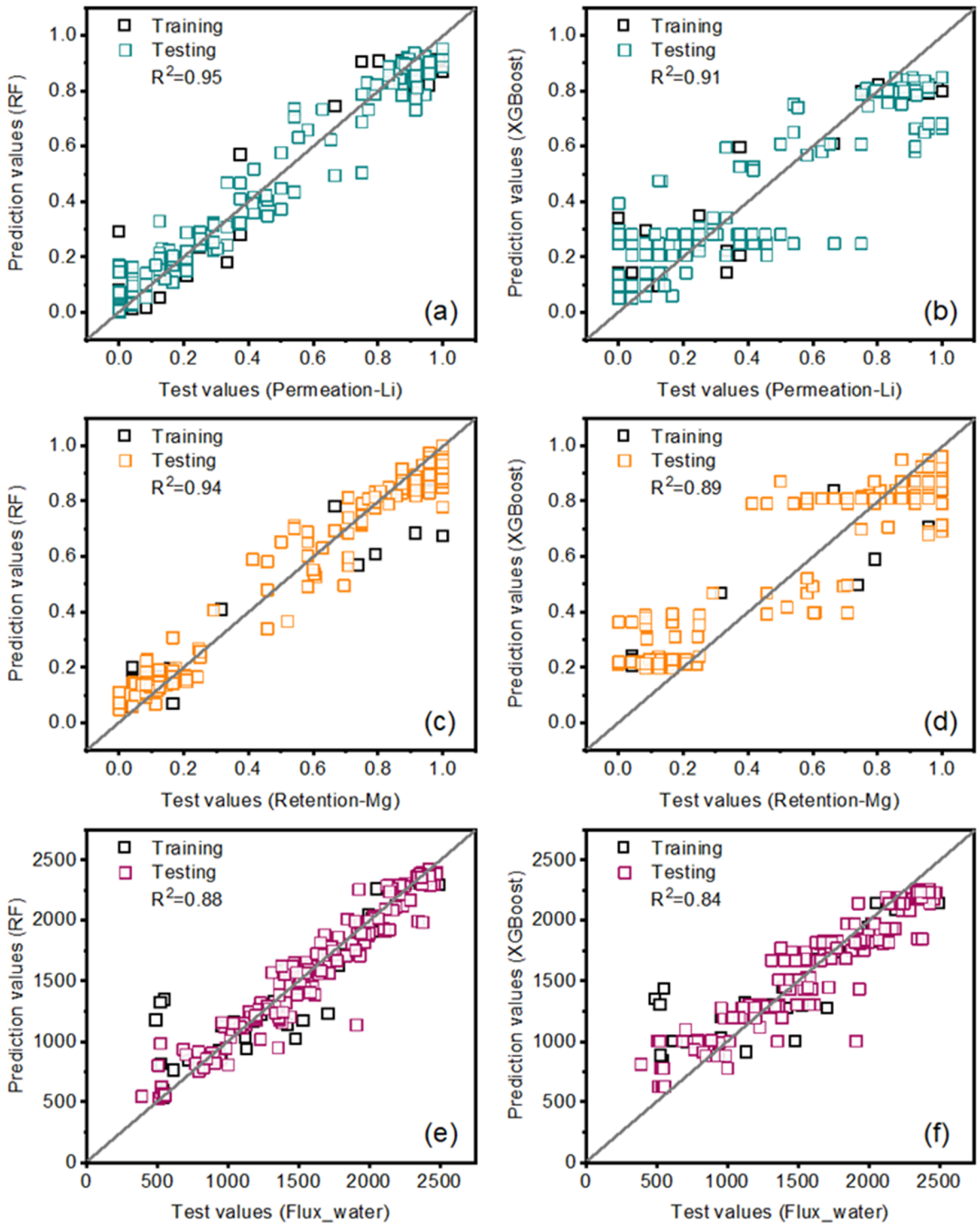

Figure 2. Comparison of RF predictions and simulation results for (**a**) P_Li^+, (**c**) R_Mg^{2+}, (**e**) Flux_water. Comparison of XGBoost predictions and simulation results for (**b**) P_Li^+, (**d**) R_Mg^{2+}, and (**f**) Flux_water.

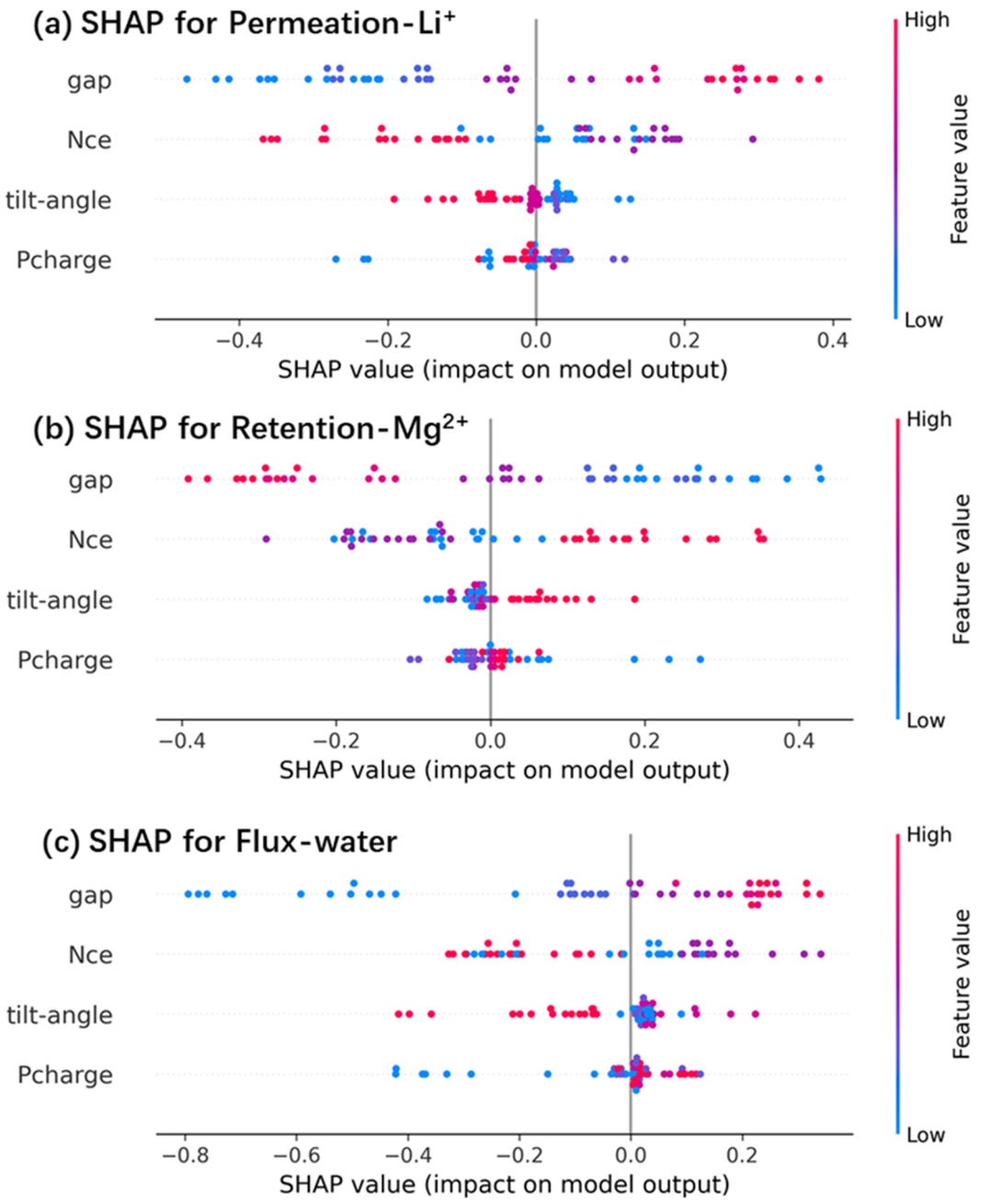

Figure 3. SHAP summary plots of the random forest model, illustrating the dependence of model predictions on membrane structure descriptors. (**a**–**c**) correspond to the model outputs for Permeation-Li^+, Retention-Mg^{2+}, and Flux-water, respectively. The SHAP value represents the contribution of each feature to the model output for individual samples, reflecting feature importance, direction of influence (positive/negative), and interaction patterns as learned from the training data.

3.3. Comparison of Pareto Optimal Solution Set and Weighting Strategy

During the actual separation process, there is an inherent trade-off relationship among the Li^+ permeability, Mg^{2+} retention rate, and water flux. Increasing one of these indicators often leads to a decrease in the others. Therefore, the optimal systems selected under different weight preferences show significant differences. Based on the three-objective prediction results of 240 sets of structural parameters using random forests, a Pareto front was constructed in the three-dimensional objective space (Flux-water, Li^+ permeation, Mg^{2+} retention). The gray points represent all systems, the green/orange points are non-dominated data, that is, the points on the Pareto front, which are the combinations of structural parameters that cannot further improve the other indicators without sacrificing at least one indicator. In short, these points represent the optimal systems selected after weighing the three objectives. It can be seen that the optimal options corresponding to the two forms of weight strategies have significant differences. In the weight 1: Li^+ permeability = Mg^{2+} retention rate = water flux, that is, the three

objectives are equally important, aiming for the balance of overall performance, as shown in Figure 4a, it is more inclined to cover the balance of overall performance, including some combinations that exchange higher water flux for medium Li^+ permeability and Mg^{2+} retention rate, reflecting the trade-off relationship between flux and selectivity; and the weight 2: Li^+ permeability = Mg^{2+} retention rate > water flux, that is, emphasizing membrane selectivity, as shown in Figure 4b, the frontier points converge significantly towards the high selectivity region, with more points clustering at the position with higher Li^+ permeability and Mg^{2+} retention simultaneously. The spatial distribution comparison of the frontier points actually shows that one is dominated by flux and the other by separation selectivity.

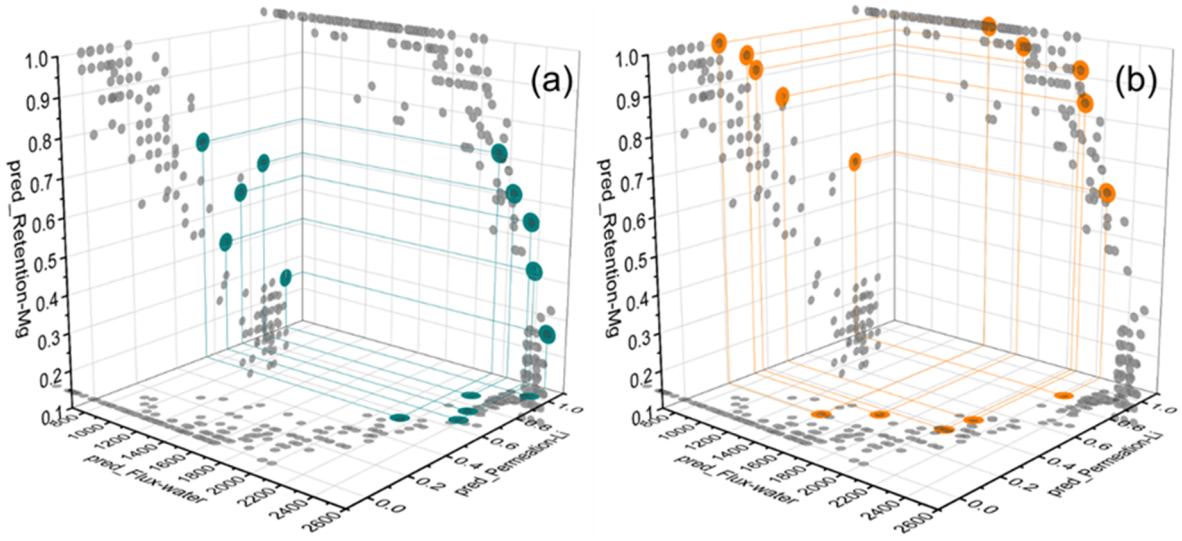

Figure 4. Comparison of Pareto front distributions derived from the random forest model predictions under different weighting strategies. (**a**) Emphasizing the balance of overall performance and (**b**) emphasizing membrane selectivity. These frontiers represent trade-offs among multiple predicted performance metrics as optimized within the model framework. The blue and orange points denote the Pareto-optimal solutions obtained under each scheme.

Using the prediction results of the RF model as the fitness function, iterative optimization is carried out through the selection, crossover, and mutation operations of the genetic algorithm. Eventually, the optimal membrane structure parameter combination is obtained: the number of CE is 1, the non-homogeneous charge of the membrane is 55%, the membrane inclination angle is 8.6°, and the interlayer spacing is 15 Å. To verify the reliability of the optimization results, the optimal structural parameters are substituted into the previous MD simulation model for dynamic simulation, and the actual performance indicators are obtained as follows: water flux = 2298 $L \cdot m^{-2} \cdot h^{-1} \cdot bar^{-1}$, Li^+ permeability = 72.4%, Mg^{2+} retention rate = 58.4%. The predicted value of the RF model for this parameter combination is: water flux = 2310.4 $L \cdot m^{-2} \cdot h^{-1} \cdot bar^{-1}$, Li^+ permeability = 70.4%, Mg^{2+} retention rate = 55.8%. The error between the predicted value and the actual value is relatively small, indicating that the optimization results are reliable, and the RF model has a high prediction accuracy.

3.4. The Synergistic Separation Mechanism of Crown Ether-Modified GO Membrane Structure

Based on multi-objective optimization analysis and combined with the RF model, the membrane structure parameter combination with superior performance was selected: the number of CE is 1, the non-homogeneous charge of the membrane is 55%, the membrane inclination angle is 8.6°, and the interlayer spacing is 15 Å. To reveal the intrinsic mechanism of how this optimal combination synergistically enhances the Li^+ permeability, the Mg^{2+} retention rate, and water flux, analysis needs to be conducted from three aspects: ion dehydration behavior, Donnan effect regulation, and channel structure synergy.

(1) The regulation of ion dehydration behavior by interlayer spacing.

The interlayer spacing is a key structural parameter affecting the energy barrier for ion transmembrane transport. The optimized interlayer spacing in this study is 15 Å, which lies between the hydration diameters of hydrated Li^+ (~7.6 Å) and hydrated Mg^{2+} (~8.6 Å), but is smaller than the characteristic size of their second hydration layers. Within this confined space, ions must undergo partial dehydration when entering the membrane channel. The radial distribution function (RDFs) of the change in hydration number before and after ions pass through the membrane channel (Figure 5) indicates that when the interlayer spacing is compressed to 15 Å, the

number of water molecules lost by Li^+ from the first hydration shell is approximately 0.5–0.8, while Mg^{2+} has a higher hydration energy and hydration number, making it difficult to remove water molecules from the first hydration shell. This difference in dehydration energy barrier gives the membrane a stronger retention ability for Mg^{2+}, while allowing Li^+ to achieve transmembrane transport with a lower energy barrier.

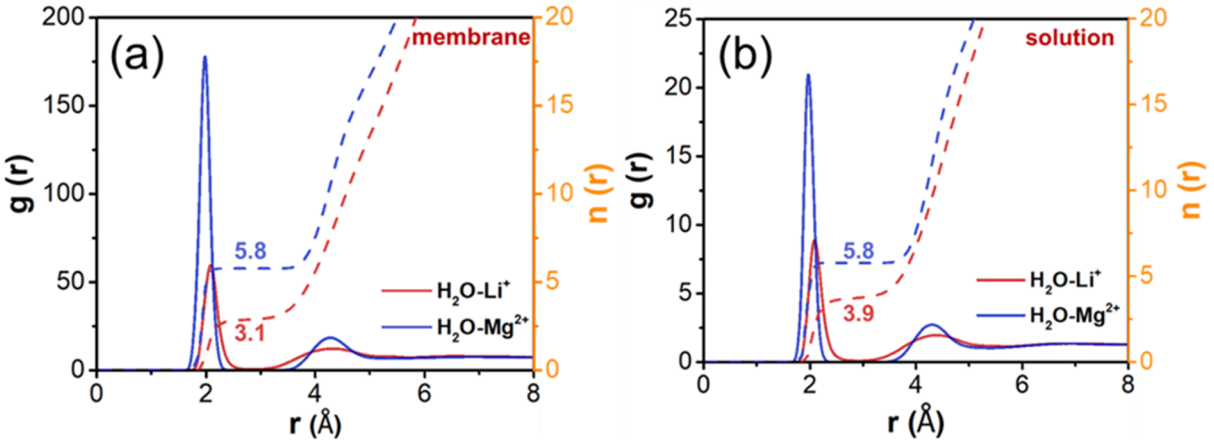

Figure 5. RDFs of Cations and Water (Oxygen Atoms) in (**a**) membrane and (**b**) solution. The dotted lines in the figure represent the coordination number.

(2) Synergistic effect of CE specificity recognition and Donnan effect.

In the optimal combination, the number of CE (15-crown-5,15C5) is 1. This moderate loading amount not only avoids excessive CE causing excessive expansion of interlayer channels (weakening the size sieving effect), but also ensures sufficient functional site density to exert specific recognition of Li^+. The cavity size of the CE closely matches the ionic radius of Li^+, and through ionic-dipole interaction, it achieves selective capture and acceleration of Li^+ transmission, forming an identification-transmission synergistic mechanism.

The coordination interaction energy between the CE site and Li^+ (−45.2 kJ/mol) is significantly higher than that with Mg^{2+} (−12.8 kJ/mol), confirming the specific recognition of Li^+ by the CE. The time required for all cations passing through the channel to enter and cross the channel during the separation process was calculated, and the average value was taken (Figure 6). On the one hand, the introduction of CE into the GO channel has shortened the time for Li^+ to enter the channel. This is due to the compensation effect of CE on Li^+ entering the channel, and the hydration structure makes Li^+ more prone to dehydration, thus making it easier for Li^+ to enter the channel. On the other hand, the introduction of CE increased the residence time of cations in the channel. Overall, the introduction of CE effectively inhibits the transport rate of Mg^{2+} while promoting the transport rate of Li^+.

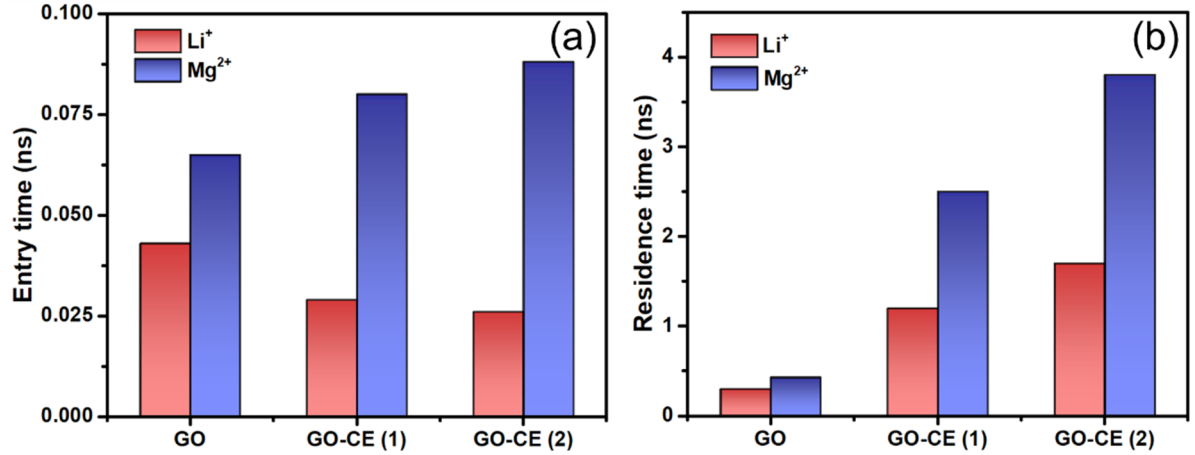

Figure 6. The average (**a**) entry time and (**b**) residence time of ions.

Meanwhile, the non-homogeneous charge of the membrane is set at 55%. This moderate non-homogeneity degree builds a local electric field gradient within the membrane. Figure 7 shows the distribution of electrostatic interaction energies between Li^+ and Mg^{2+} and the membrane surface under two conditions: the original GO membrane and the non-homogeneous GO membrane (non-homogeneous charge of 55%). The results show that

compared with the homogeneous GO membrane, the charge of the non-homogeneous GO membrane increases the electrostatic repulsion energy of Mg^{2+} from −12.3 kJ/mol to −18.7 kJ/mol (i.e., the absolute value increases), while that of Li^+ only changes from −5.1 kJ/mol to −6.4 kJ/mol. During the separation process, the non-homogeneous charge distribution on the membrane surface and between layers strengthens the Donnan repulsion effect, exerting a stronger electrostatic repulsion effect on the high-valent Mg^{2+}, while the repulsion on the low-valent Li^+ is relatively weaker. The recognition effect of the CE and the Donnan repulsion effect form a positive synergy: the CE site guides Li^+ to enter the channel first, and the non-homogeneous charge layer further inhibits the transmembrane transmission of Mg^{2+}, ultimately achieving the simultaneous improvement of high Li^+ permeability and high Mg^{2+} retention rate.

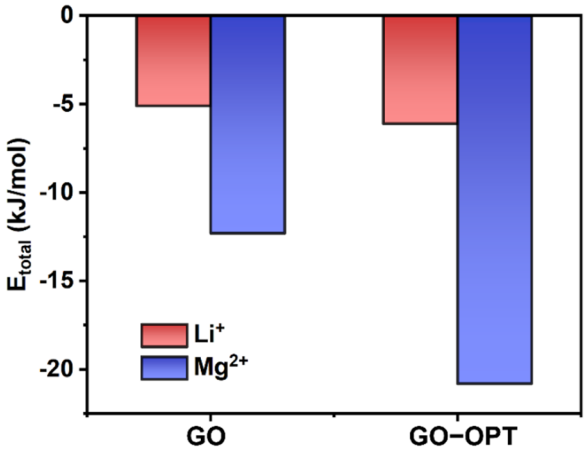

Figure 7. The electrostatic interaction energy between Li^+ and Mg^{2+} and the membrane surface.

(3) The optimization of channel configuration and transmission path by tilt angle.

The optimal combination has a membrane inclination angle of 8.6°. This small inclination angle maintains the connectivity of the interlayer channels while introducing a moderate degree of channel curvature. Compared to the completely parallel stacking (0°) or structures with a larger inclination angle (≥10°), an inclination angle of 8.6° achieves optimization in the following two aspects: Firstly, it avoids excessive distortion of the interlayer channels caused by large-angle inclination, maintaining the rapid transmission channels for water molecules and Li^+; Secondly, the moderate channel curvature increases the transmission path length and collision probability of Mg^{2+}, prolonging the interaction time with the charged channel wall and CE sites, further enhancing the retention efficiency. The channel configuration under this inclination angle achieves the best balance between mass transfer efficiency and separation selectivity. The Li^+ transmission trajectory further confirms this point (Figure 8). Compared with the original GO, the residence time of Li^+ in the GO-OPT channel is significantly shortened, indicating that the membrane tilt angle of 8.6° is conducive to the further transmission of Li^+ in the channel, thereby improving the overall Li^+ transmission efficiency.

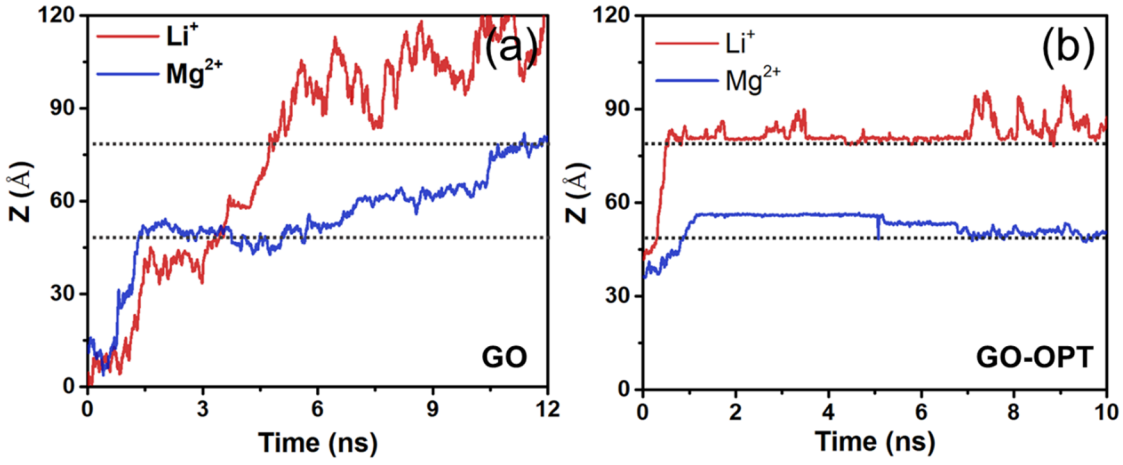

Figure 8. The trajectory of Li^+ and Mg^{2+} in the Z-direction changing with time in different channels, (**a**) GO and (**b**) GO-OPT.

(4) Realization of optimal performance through multi-parameter synergy.

The four structural parameters mentioned above do not act independently but are jointly determined by the overall separation performance of the membrane through a complex synergy mechanism. The interlayer spacing lays the foundation for size sieving selectivity; the number of CE provides the chemical recognition function; the heterogeneous charge distribution regulates the strength of electrostatic repulsion; the inclination angle optimizes the channel transmission structure. Through the synergistic effects of these four factors, the permeability of Li^+ and the retention rate of Mg^{2+} can be simultaneously improved.

To verify the reliability of this optimization mechanism, the optimal structural parameters were substituted into MD simulations for verification. The actual performance obtained from the simulation was in good agreement with the predicted values of the RF model (relative error of water flux: 0.5%, relative error of Li^+ permeability: 2.8%, relative error of Mg^{2+} retention rate: 4.5%). This further confirmed the rationality of the above mechanism analysis. This optimal structure combination provides a clear theoretical basis and experimental reference for the rational design and performance optimization of CE-modified GO membranes.

4. Conclusions

This study employed machine learning methods to construct a model for predicting the separation performance of functionalized graphene oxide membranes. Through feature importance analysis and parameter optimization, the relationship between membrane structural parameters and separation performance was deeply explored. The main conclusions are as follows:

Both the RF and XGBoost models can effectively predict the membrane separation performance, with RF showing stronger predictive performance on the test set. The R^2 value of the RF model for water flux is 0.881, for Li^+ permeability is 0.950, and for Mg^{2+} retention rate is 0.943. It can effectively describe the complex nonlinear correlation between structural parameters and performance. In terms of the influencing rules, water flux is mainly controlled by interlayer spacing and membrane inclination angle, increasing the spacing and reasonably regulating the inclination angle is conducive to improving the flux; Li^+ permeability is determined by interlayer spacing and the number of CE molecules, and the combined effect of the two can significantly enhance ion transport; while Mg^{2+} retention rate mainly depends on the number of CE grafts and the non-uniform charge of the membrane, which reflects the synergistic regulatory effect of the Donnan effect and specific recognition. There are obvious interactive influences among the structural parameters, for example, the number of CE molecules and interlayer spacing can synergistically enhance Li^+ permeability, the number of CE molecules and charge can couple to enhance the Mg^{2+} retention effect, further confirming the ion separation mechanism proposed in the previous text. On this basis, through multi-objective optimization, two membrane structure schemes with different emphases were obtained. The scheme with the best comprehensive performance can ensure high selectivity while also considering flux, and has good practical application potential.

This study combines machine learning methods with traditional membrane separation research, not only improving the research efficiency, but also deeply exploring the intrinsic structure–performance relationship, providing new ideas for the design and optimization of high-performance lithium separation membrane materials. Future research can further expand the dataset size, introduce more advanced machine learning algorithms, such as deep learning and transfer learning, to further improve prediction accuracy and generalization ability. At the same time, machine learning can be combined with experimental design to achieve efficient development and optimization of membrane materials.

Author Contributions

M.G.: conceptualization, investigation, visualization, writing—original draft, Writing—review & editing; C.W.: investigation; Y.S.: methodology, data curation, formal analysis: T.F.: conceptualization, formal analysis, software, validation, supervision, resources, funding acquisition; X.L.: project administration, resources, funding acquisition. All authors have read and agreed to the published version of the manuscript.

Funding

This work was financially supported by the National Natural Science Foundation of China (22108139, 22178187); Natural Science Foundation of Shandong Province (ZR2021MB006); Taishan Scholars Program of Shandong Province (tsqn201909091); Open Research Fund of School of Chemistry and Chemical Engineering, Henan Normal University (2024Y10); the High-Grade Talents Plan of Qingdao University.

Institutional Review Board Statement

Not applicable.

Informed Consent Statement

Not applicable.

Data Availability Statement

The datasets generated during the current study are not publicly available because they form part of an ongoing research project and may be used in future publications. However, data supporting the conclusions of this work are available from the corresponding author upon reasonable request.

Conflicts of Interest

The authors declare no competing financial interest.

Use of AI and AI-Assisted Technologies

No AI tools were utilized for this paper.

References

1. Wei, C.; Wang, Y.; Ding, Z.; et al. A Universal Strategy toward Low-Cost Aqueous Sulfur–Iodine Batteries. *Adv. Funct. Mater.* **2023**, *33*, 2212644.
2. Chen, K.; Li, F.; Wei, T.; et al. An Interlayer-Based Positive Charge Compensation Strategy for the Preparation of Highly Selective Mg^{2+}/Li^{+} Separation Nanofiltration Membranes. *J. Membr. Sci.* **2023**, *684*, 121882.
3. Wang, Q.; Song, J.; Gao, X.; et al. Carbon Nanotube Membranes for the Separation of Li^{+} and Mg^{2+} Ions: Effect of Functional Groups with Charges. *Desalination* **2022**, *540*, 115996.
4. Grosjean, C.; Miranda, P.H.; Perrin, M.; et al. Assessment of World Lithium Resources and Consequences of Their Geographic Distribution on the Expected Development of the Electric Vehicle Industry. *Renew. Sust. Energ. Rev.* **2012**, *16*, 1735–1744.
5. Razmjou, A.; Asadnia, M.; Hosseini, E.; et al. Design Principles of Ion Selective Nanostructured Membranes for the Extraction of Lithium Ions. *Nat. Commun.* **2019**, *10*, 5793.
6. Geng, H.; Peng, Y.; Qu, L.; et al. Structure Design and Composition Engineering of Carbon-Based Nanomaterials for Lithium Energy Storage. *Adv. Energy Mater.* **2020**, *10*, 1903030.
7. Wang, W.; Wang, C.; Huang, R.; et al. Boosting Lithium/Magnesium Separation Performance of Selective Electrodialysis Membranes Regulated by Enamine Reaction. *Water Res.* **2025**, *268*, 122729.
8. Zhai, J.; Balogun, A.; Bhattacharjee, S.; et al. Nanofiltration as Pretreatment for Lithium Recovery from Salt Lake Brine. *J. Membr. Sci.* **2024**, *710*, 123150.
9. Peng, H.Y.; Lau, S.K.; Yong, W.F. Recent Advances of Thin Film Composite Nanofiltration Membranes for Mg^{2+}/Li^{+} Separation. *Adv. Membr.* **2024**, *4*, 100093.
10. Li, X.; Mo, Y.; Qing, W.; et al. Membrane-Based Technologies for Lithium Recovery from Water Lithium Resources: A Review. *J. Membr. Sci.* **2019**, *591*, 117317.
11. Zhang, C.; Mu, Y.; Zhao, S.; et al. Lithium Extraction from Synthetic Brine with High Mg2+/Li+ Ratio Using the Polymer Inclusion Membrane. *Desalination* **2020**, *496*, 114710.
12. Zhang, Y.; Wang, L.; Sun, W.; et al. Membrane Technologies for Li+/Mg2+ Separation from Salt-Lake Brines and Seawater: A Comprehensive Review. *J. Ind. Eng. Chem.* **2020**, *81*, 7–23.
13. Jie, K.; Onishi, N.; Schott, J.A.; et al. Transforming Porous Organic Cages into Porous Ionic Liquids Via a Supramolecular Complexation Strategy. *Angew. Chem. Int. Ed.* **2020**, *59*, 2268–2272.
14. Christy, F.A.; Shrivastav, P.S. Conductometric Studies on Cation-Crown Ether Complexes: A Review. *Crit. Rev. Anal. Chem.* **2011**, *41*, 236–269.
15. Ali, M.; Ahmed, I.; Ramirez, P.; et al. Lithium Ion Recognition with Nanofluidic Diodes through Host–Guest Complexation in Confined Geometries. *Anal. Chem.* **2018**, *90*, 6820–6826.
16. Ge, M.; Wei, C.; Fang, T.; et al. Molecular Insight into the Separation Mechanism of Crown Ether-Based Channels for Lithium Extraction. *Sep. Purif. Technol.* **2024**, *338*, 126415.
17. Ge, M.; Wang, D.; Wei, C.; et al. Insight into the Separation Mechanisms of MXene@PSS Nanochannels for High-Efficiency Lithium Extraction. *Sep. Purif. Technol.* **2025**, *363*, 132082.
18. Ge, M.; Wei, C.; Meng, L.; et al. Insight into the Separation Mechanisms of High-Efficiency Lithium Extraction Based

on Janus Membrane with Heterogeneous Charge. *Chem. Eng. Sci.* **2026**, *326*, 123504.
19. Liang, L.; Lu, D.; Qin, Y.; et al. Machine Learning in Membrane Science: Bridging Materials, Structures, and Performance for Next-Generation Membrane Design. *Sep. Purif. Technol.* **2025**, *369*, 133091.
20. Ji, Z.; Guan, H.; Wang, M.; et al. Polymeric Membrane Concentration of Lithium-Magnesium Solution for Sustainable Resource Recovery with Machine Learning. *Water Res.* **2025**, *287*, 124438.
21. Cao, J.; Xu, Z.; Wei, M.; et al. New Insights into Li+/Mg2+ Separation by a Cnt Model Membrane Via Coupling High-Throughput Simulations and Machine Learning. *J. Membr. Sci.* **2026**, *738*, 124870.
22. Wu, T.; Zhang, J.; Yan, Q.; et al. Machine Learning in the Design and Performance Prediction of Organic Framework Membranes: Methodologies, Applications, and Industrial Prospects. *Membranes* **2025**, *15*, 178.
23. Lu, D.; Ma, X.; Lu, J.; et al. Ensemble Machine Learning Reveals Key Structural and Operational Features Governing Ion Selectivity of Polyamide Nanofiltration Membranes. *Desalination* **2023**, *564*, 116748.
24. Sun, J.-O.; Hua, T.-W.; Guan, Y.-F.; et al. Predicting and Understanding the Performance of Polyamide Nanofiltration Membrane for Li/Mg Selective Separation Based on Machine Learning. *Water Res.* **2025**, *285*, 124140.
25. Bonnet, N.; Marzari, N. Ion Sieving in Two-Dimensional Membranes from First Principles. *ACS Nano* **2025**, *19*, 8552–8560.
26. Ignacz, G.; Bader, L.; Beke, A.K.; et al. Machine Learning for the Advancement of Membrane Science and Technology: A Critical Review. *J. Membr. Sci.* **2025**, *713*, 123256.
27. Wu, J.; Li, N.; Liu, S.; et al. Graphene Oxide Membranes with a Confined Mass Transfer Effect for Li^+/Mg^{2+} Separation: A Molecular Dynamics Study. *Phys. Chem. Chem. Phys.* **2022**, *24*, 26011–26022.
28. Zhang, N.; Yu, H.; Zhang, J.; et al. Pressure-Driven Li^+/Mg^{2+} Selective Permeation through Size-Sieving Nanochannels: The Role of the Second Hydration Shell. *Sep. Purif. Technol.* **2023**, *327*, 124818.
29. Plimpton, S. Fast Parallel Algorithms for Short-Range Molecular Dynamics. *J. Comput. Phys.* **1995**, *117*, 1–19.
30. Berendsen, H.J.C.; Grigera, J.R.; Straatsma, T.P. The Missing Term in Effective Pair Potentials. *J. Phys. Chem.* **1987**, *91*, 6269–6271.
31. Li, P.; Song, L.F.; Merz, K.M., Jr. Systematic Parameterization of Monovalent Ions Employing the Nonbonded Model. *J. Chem. Theory Comput.* **2015**, *11*, 1645–1657.
32. Li, P.; Roberts, B.P.; Chakravorty, D.K.; et al. Rational Design of Particle Mesh Ewald Compatible Lennard-Jones Parameters for +2 Metal Cations in Explicit Solvent. *J. Chem. Theory Comput.* **2013**, *9*, 2733–2748.
33. NosÉ, S. A Molecular Dynamics Method for Simulations in the Canonical Ensemble. *Mol. Phys.* **2002**, *100*, 191–198.
34. Pirbonyeh, M.A.; Shayegan, M.A. Influence of Feature Normalization Methods on Transfer Learning—A Comparison Study. *Multimed. Tools Appl.* **2025**, *84*, 48811–48847.
35. Mathivanan, N.M.N.; Xian, E.F.Z.; Xi, D.F.Y.; et al. Impact of Feature Standardization on Heart Disease Prediction: A Comparative Analysis of Logistic Regression and Support Vector Machine Models. *Malays. J. Comput.* **2025**, *10*, 2159–2175.
36. Bui, N.T.; Savova, G.K.; Wang, L. In *Assessing the Macro and Micro Effects of Random Seeds on Fine-Tuning Large Language Models, Proceedings of the 14th International Joint Conference on Natural Language Processing and the 4th Conference of the Asia-Pacific Chapter of the Association for Computational Linguistics, Mumbai, India, 20–24 December 2025*; The Asian Federation of Natural Language Processing and The Association for Computational Linguistics: Mumbai, India, 2025; pp. 41–46.
37. Zhang, Y.; Han, B.; Song, Q.; et al. Revealing Key Structural and Operating Parameters on Salt/Dye Separation of Loose Nanofiltration Membrane by Ensemble Machine Learning. *J. Membr. Sci.* **2025**, *732*, 124274.
38. Gao, K.; Deng, S.; Liu, S.; et al. Interpretable Machine Learning for Predicting Separation Performance of Mofs Membrane and Suppressing Permeability-Micropollutant Rejection Trade-Off. *J. Membr. Sci.* **2026**, *748*, 125345.
39. Altman, N.; Krzywinski, M. Ensemble Methods: Bagging and Random Forests. *Nat. Methods* **2017**, *14*, 933–934.
40. Schalk, D.; Bischl, B.; Rügamer, D. Accelerated Componentwise Gradient Boosting Using Efficient Data Representation and Momentum-Based Optimization. *J. Comput. Graph. Stat.* **2023**, *32*, 631–641.
41. Chicco, D.; Warrens, M.J.; Jurman, G. The Coefficient of Determination R-Squared Is More Informative Than Smape, Mae, Mape, Mse and Rmse in Regression Analysis Evaluation. *PeerJ Comput. Sci.* **2021**, *7*, e623.
42. Lundberg, S.M.; Lee, S.-I. A Unified Approach to Interpreting Model Predictions. In *Proceedings of the 31st International Conference on Neural Information Processing Systems*; Curran Associates Inc.: Long Beach, CA, USA, 2017; pp. 4768–4777.
43. Aas, K.; Jullum, M.; Løland, A. Explaining Individual Predictions When Features Are Dependent: More Accurate Approximations to Shapley Values. *Artif. Intell.* **2021**, *298*, 103502.
44. Yogarathinam, L.T.; Abba, S.I.; Usman, J.; et al. Interpretable Shap-Based Machine Learning-Assisted Design for Selecting Ultrafiltration Membranes in Protein-Laden Phosphate Wastewater. *Clean. Chem. Eng.* **2025**, *11*, 100187.